Flood susceptibility in urban environment using multi-layered neural network model from satellite imagery sources

Swathika R.[1]*, Radha N.[1], Sasirekha S.P.[2] and Dhanabal S.[3]

[1]Department of Information Technology Sri Sivasubramaniya Nadar College of Engineering, Chennai, Tamil Nadu, India

[2]Department of CSE, Karpagam academy of higher education, Eachanari, Coimbatore, Tamil Nadu, India
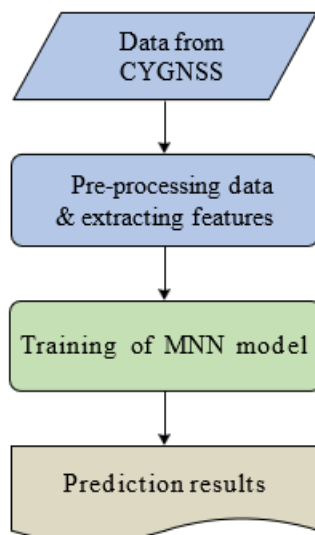
[3]Department of CSE, Kongunadu College of Engineering and Technology, Trichy, Tamil Nadu, India

*to whom all correspondence should be addressed: e-mail: swathikar@ssn.edu.in

Graphical abstract

Abstract

Recently, there has been a rise in research based on data-driven based machine learning models to address the issue of processing speed posed by various physiological simulations. The majority of studies, however, have concentrated on creating models for particular water sources, drainage systems, and gauge stations area. Therefore, unless further data is supplied and the models are subsequently trained, their outcomes cannot be effectively applied to different scenarios. With its excellent spatio-temporal accuracy range with the advanced analytics, the forthcoming Global Navigations Satellite Systems (GNSSs) technology offers a novel method for the monitoring of flood disasters in dynamic manner. This study recommends a Multi-layered Neural Network (MNN) for flood monitoring, which combines a Convolutional Neural Networking (CNN) along with a backward propagation based (BP) learning network. The CNN component is used to obtain the abstracted features from full delay doppler maping images. The BP section is provided with GNSSs characteristics, such as reflection of surface with power range, and also the vegetation attributes from the Soil Moistening Active Passives (SMAP) satellite source data. In comparison to physiologically based models, the results shown that the CNN-oriented system makes accurate predictions on "unseen" areas of catchment with a substantially shorter processing time. The obtained results imply that, with respect to accuracy of prediction, the patch-enabled option is superior to the resizing-based option. Additionally, every experiment has demonstrated that the forecast of flow speed is more precise than the prognosis of water depth, indicating that the water deposition is more complex to information about global level elevations than the flow speed with velocity.

1. Introduction

The East Asian areas border the North Pacific to progressively hit by a greater number of disastrous flood catastrophes as a direct result of the bigger and more powerful storms. ANNs models be effective and quickly forecasting river system floods in limited locations (Nevo *et al*., 2019; Salas *et al*., 2018). In Japan, typhoon- & heavy-rainfall-prone areas have seen river system disasters in the last 3–4 years (Realestate Blog, 2019). Most important Japanese rivers have real-time overflow-risk detection. However, a quick-response effective flood technology that can foresee has not yet been put into practice in particular river sites. Utilizing flood detection systems, humans are ready to terminate a disaster. As a result, there could have been fewer casualties. A deep learning-enhanced ANN model is a contender when a prediction flood forecasting system is created for usage in real-world scenarios owing to the model's characteristics. The ANNs data-driven it lacks physics-based on metrics sets. For instance a rainfall-runoff models must be validated in a given area (Tokar *et al*., 2000). A physical model, like the rainfall-runoff model, needs many studies.

Depending only on previous data learning, the ANN model is capable of predicting a near-future trend. ANN predictions has minimal starting intricacy but advancement cost. The ANN-based flood model's primary advantages lie in its speedy reaction to the warning signs of a flood that will occur in the not-too-distant future and its straightforward execution using just historical data (Akhtar *et al*., 2009). ANNs approach has been used to forecast floods (Maier *et al*., 2010). ANN models using deep learning are used to forecast floods (Hitokoto *et al*., 2016). The LSTMs design (Hochreiter and Schmidhuber, 1997; Gers *et al*., 1999). were employed to evaluate the soil moisture in flooding (Yamada *et al*., 2016; Hu *et al*., 2018; Le *et al*., 2019).

In the majority of case reports, ANN models predicted exactly previous flood occurrences using a variety of datasets. ANN models often demand substantial computing expenses throughout the training procedure because of massive datasets. To decrease computing costs, we use transfer learning (Pratt, 1992). In a raw input that might be applied to other target areas, approaches were built using big datasets. Following a part regarding the pre-trained model's–training using target datasets, the trained and certified technique may deliver suitable results at a relatively minimal cost. The work concentrate on forecasting time information, such as water levels, for flood occurrences. The ideal method for processing time-series data is to use an LSTM architecture integrated into an ANN model. Deep learning and LSTM have been created. (Laptev *et al*., 2018) found that LSTMs with transfer training decreased inefficiencies in long-term U.S. electric energy consumption patterns. However, LSTM has typically not proven effective, particularly for short-term, quickly changing, and non-periodic data, like data on flood waves. The following explanation fits this finding: Rarely can an unpredictable life value be predicted as from an exact value (Potikyan, 2019).

For 2D-spatial image recognition, CNN (LeCun *et al*., 1998) is utilized. CNNs implementation with an ANNs model generated strong transfer learning outcomes (Kensert *et al*., 2019; Kolar *et al*., 2018). A new picture database is often classified using ImageNet (Visual Geometry Group, 2019), and created using VGG16. Because it sequentially integrates from basic visual qualities on a bottom layer to data source knowledge representation on a protocol stack, CNNs with the proposed method perform well (Preethi and Asokan, 2020; Zeiler and Fergus, 2014). We came to the conclusion that a CNNs enhanced with deep learning is more reliable and practical than an LSTMs enhanced with supervised learning. Converting time information to image information for an ANNs model is tricky. How to depict time-series structures in 2D has been studied. 31 stocks were employed across 100-time intervals to estimate the near-term share market (Miyazaki and Matsuo, 2017). Data sets on geographical meteorological data, such as thermal effects at 8 places, were utilized to predict moisture in ten-minute intervals and eight-time scales (Suzuki *et al*., 2018). CNNs and transfer learning may forecast flood data via conversions

A brand-new data-driven hydrological models were created in this study. The planned work's contributions are,

- The approach integrates a CNNs with domain adaptation to anticipate time-series groundwater table in floods even within multiple areas acquiring CNNs methods in a single domain
- The CNN-based flooding model's efficiency is used with strong data restoration capacity.
- Reducing computational costs and Root mean squared error increased CNN classification technique.

2. Related Works

Researchers& disaster strategists have focused relating to flood predictions and alert technologies to lessen disasters and to plan effective responses. The modern techniques for preventing flooding over the last ten years are listed in Table 1. ANN is often used for flood prediction (Preethi and Asokan, 2021). (Sankaranarayanan *et al*., 2020) employed a deep neural network for speculating about floods. Training a multilayer ANN model that might predict a potential flood occurrence, the scientists utilized meteorological information including temperature and rainfall intensity. These models can evaluate the possible harm that severe rains might do to houses, buildings, and infrastructures. Similar to this, (Preethi and Asokan, 2019) utilized many hidden layers as opposed to in their ANN model, there is one, which produced results with much greater accuracy than a conventional ANN model. The zones of clouds, land, and water were independent of the satellite measurements using SVM, which resulted in overall classification results of 92% for their proposed floodplain mapping system. Their research is constrained, nonetheless, by the use of noise- and weather-dependent remotely detected images. Additionally, in darker areas like building foundations, behind bridges, and other covered areas, such photos cannot be taken. This reliance prevents the user from initiating rapid crisis actions because clouds are frequently present during rain-related floods.

Elsafi (2014) employed an ANN model to predict flood events using upstream data from the Nile River in Sudan. A learnt ANN model was used to recreate the flows at particular river locations using data from upstream sites in order to forecast the occurrence of floods. Anusha and Bharathi (2020) investigated flood identification and modeling was employed as image processing method like factorizing to distinguish water patches from the input pictures. The SAR photographs of the target region were used to compile the dataset. To eliminate speckle noise from pictures, a median filter and image rectification were used. Every image was classified as "water" or "non-water" using a pixel-based threshold. Similar findings were seen in research by (Preethi and Asokan, 2019), where the suggested CNN architecture increased the statistic from 0.615 to 0.687 in comparison to its monitored equivalent. Improved accuracy for flood-affected open areas (FO) (0.506-0.684) reduces recall

(from 0.842 to 0.824), but both improve for FB. In different research (Zhao *et al.*, 2020), CNN outperformed the SVM and RF with an accuracy of 0.91 for CNN & 0.89 for LeNet-5 during the testing phase. (Hosseiny *et al.*, 2020) employed RFs for flood prediction and the MLP model for depth detection. For depth, the MLP model produced a regression coefficient of 0.89, while RF technique produced a detection accuracy of 98.5% for the flooded areas. Because of this, the cost of computations in mechanical or hydraulic modeling may be decreased by using this much less sophisticated technique to learn algorithms.

Other studies stressed "warning communities" as a means of mitigating the disastrous impacts of floods and centered their attention on the usage of alert systems in flood conditions (Basha and Rus, 2007). A flash flood forecasting structure relies on a statistical model and uses a threshold occurrence mechanism during heavy downpours was developed by (Alfieri *et al.*, 2011). A rain index was also created. The flood level is measured and estimated using computer vision from photographs that have been collected by (Preethi *et al.*, 2021). People in the disaster zone might take pictures of these things and upload them to the server. For data processing of the picture, the scientists used the SIFT techniques. In planning an efficient disaster response, geo-tagging data was used to determine the region's geographic location. Flood sensor nodes are often used by (Mousa *et al.*, 2016) to evaluate the level of flood waters using an ultrasonic distance locator and condition monitoring.

The data from the sensor was analysed using the ANN approach to determine the water level in significant buildings, homes, and smart structures. Numerous studies have built and employed artificial intelligence (AI) systems to control risks by extracting data from social media (Wang *et al.*, 2018; Smith *et al.*, 2017). The emergency response has been sparked by status updates, image uploads, and opinions. AI algorithms have been trained to recognise these images and comments and to provide aid to the affected locations. Facebook employs CNN for tagging face identification, while Google does the same (Amit and Aoki, 2017). Numerous applications of UAVs have been studied and employed, including smart real estate investment (Ullah *et al.*, 2018; Felli *et al.*, 2018), intelligent buildings (Zhao *et al.*, 2020), smart healthcare (Islam and Shin, 2020), and many more. UAVs are used for disaster risk management, post-disaster phase transition using IoT, public security in disaster and crisis response, energy-efficient work scheduling and physical evaluation, and flood protection (Kumar *et al.*, 2020; Ejaz *et al.*, 2020; Mehallegue *et al.*, 2020). Various machine-learning methods have also been investigated for effective UAV-based flood catastrophe control. Programs like ANN, CNN, SVM, segmentation methods, and others (Kastridis *et al.*, 2020; Liu *et al.*, 2020; Rottondi *et al.*, 2021) are examples of advanced solutions.

In the newest study (Khosravi *et al.*, 2020), CNN applications in UAV-based flood catastrophe management are highlighted. UAVs may fly anywhere and gather data, including images and actual harm evaluation. CNN has

being utilised by UAVs to extract photos and videos for real-time flood assessments, as well as to assess flood damage to buildings, companies, and infrastructure (Ali and Choi, 2019; Ahmed *et al.*, 2020). The current study examines Applications developed by CNN for handling after-flood catastrophes, planning an immediate response to begin rescue efforts, and recognizing significant infrastructure damage. CNN has been used in several flood research studies. (Mason *et al.*, 2010) carried out research in which social media-posted photos of floods were put into embedded metadata to identify flood trends. To extract visual data from social media images, the CNN technique was applied to a trained ImageNet. Using word embedding, metadata provided textual data to a bidirectional RNN. Additionally, the word embedding was determined using glove vectors. The finalised images and text were then combined to provide a product with pertinent information about the disaster (Martino *et al.*, 2007) built a social media flood detection, retrieval, and visual and content analysis AI system. Cropping and pre-filtering the photos based on linguistic and chromatic information were part of the pre-processing. Lopez-Fuentes (Lopez-Fuentes *et al.*, 2017) gathered disaster photographs and located the flood using the CNN approach using the Relation Network. To paraphrase a phrase that was used on CNN recently (Zha *et al.*, 2015). In order to arrange the video and extract its spatiotemporal properties, the authors used systematic investigation. Nearby video input segment stacks and convolution layers are used in 3D-CNN research (Ji *et al.*, 2013).

Two distinct CNN models with diverse inputs were used in the two-stream technique to regulate the spatial and temporal aspects of the video (Simonyan and Zisserman, 2014). One input was an RGB picture for acquiring fractal dimension another was several frames with dense optical flow for temporal features. The final visual output is obtained by evaluating the weights of the two streams. Ye *et al.* (2015) employed the same two streaming neural network techniques and evaluated them using parameters, fusion, and predictions. Various image segmentation approaches have been applied during the last few years. These techniques classify images based on context and local information. First, the pixels are integrated into bigger-picture objects since a single pixel cannot convey exact semantic information (Sande *et al.*, 2003). The texture, size, and proximity of the picture are taken into account to extend the pixels into objects (Baatz and Schäpe, 2000). FCN models are utilized to segment conventional aerial images (Marmanis *et al.*, 2016; Sherrah, 2016). High-resolution satellite pictures were characterized using the FCN framework by (Fu *et al.*, 2017), who determined that the accuracy, recall, and kappa coefficients were significant at 0.81, 0.78, and 0.83, respectively. While classifying satellite photos, (Nguyen *et al.*, 2013) created a five-layered network technique that, on average, had an 83% classification accuracy. Another experiment attained 91% accuracy using the Cafenet and GoogleNet CNN architectures. These were used with the three different learning modalities required to classify the

land use pictures that RS had taken (Castelluccio *et al*., 2015).

DL applications using spectral data have shown higher categorization than SVM (Xue *et al*., 2020). It investigated the potential of SVM and convolutional neural networks for flood forecasting. Rainfall intensity and temperatures are utilized to train. The DNN had an efficiency of 91.18%, whereas the SVM had a reliability of 85.57%, as per the data. In another research, CNN outperformed SVM and random forest in identifying land use from RGB pictures (Jozdani *et al*., 2019).

According to the literature, deep learning models are more effective than conventional image processing and artificial intelligence techniques for picture retrieval,

categorization, and segmentation. As a result, the current work uses CNN and deep learning to identify floods using UAV aerial data. In order to develop effective and efficient disaster response plans, it is important to improve performance and research the application of machine learning for flood predictions. In order to extract visual features, modern UAVs have parallel processing and built-in FPGS. Because of PL, CNN is frequently employed to improve picture segmentation, feature categorization, and texture categorization. The current study's recommended approach, the CNN method, is also very speedy and reliable

Table 1. Recent Flood Management work overall view

Methods	Focus	Metrics	De Metrics
DNNs	Prediction of Flood	More accuracy compared to conventional ANNs.	The dataset is old. Entries from 1992 to 2002 are included.Distributional imbalance in the information were not taken into account.
ANNs	Flood Plain & Maps	More than 90% overall recognition efficiency	Noisy information being present in the training database.Older than average data (1965–2003).
SVMs	Prediction of Flood	Less time is needed to analyze the data, which reduces the cost of evaluation.	Utilize one factor for train; good when there's little data.
Image Segmentation	Flood recognition & Maps	For flood analysis and design, the identification of drowned zones could be a important element.	A large quantity of trees causes the method's processing to be extremely slower.
RFs & MLPs	Flood recognition & Flood intensity techniques	The cost of large-scale hydraulic simulators has decreasedusing mls in combination	Not feasible programs that demand real-time forecasts.
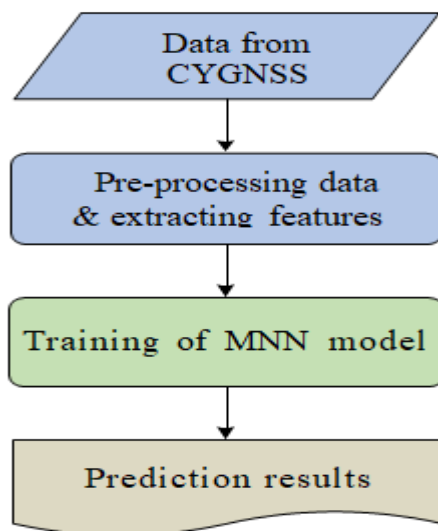
Figure 1. Overall flow of the research

2.1. Proposed methodology for flood prediction in catchment area

In order to anticipate floods, this research suggests a MNN system that blends CNN with BPML. In this approach, 2D DDMs are fed into the CNNs, which essentially populates abstractions features from images, while the BPNNs is fed seven typical GNSS-R properties, include mentioned together with these indications (Hochreiter, 1998), quality factor (Kratzert *et al*., 2019),

the front of slopes (Tan *et al*., 2018), etc., as well as plant info using SMAP databases (Long *et al*., 2015). The likelihood that DDMs reside in the submerged area is represented by the model's reported findings. The suggested technique entails the following three steps: (1) condition characterized and characteristics retrieval; (2) developing and training a MNN model; and (3) MNN model prediction. Figure 1 shows the technique.

2.2. Data pre-processing and features extraction

Only CYGNSS information that meets these parameters is used in this investigation to assure reliable reversal outcomes.

- If DDM's SNR is too low, the signal-to-noise ratio is low. To filter out the DDMs, the SNR must be inferior to 1.5 dB.

- The fraction of signals with a left-handed circular polarisation quickly drops as the incidence angle increases, hence DDMs with incident angles greater than 65 are filtered out during this analysis (Chen *et al*., 2013; Chow *et al*., 1988).

- This research exclusively uses DDMs with transmitting and receiving antenna gains larger than 0 (Leit *et al*., 2018).

- Since peak areas migrate towards to the boundaries of DDMs with altitudes and CYGNSS's DTU10 topographic maps modeling doesn't effectively compensate for land topography, the

projected placements of exceptional places higher than 600 m are imprecise. The DDMs with highest frequencies between 7 and 10 squares are maintained as a result. Due to thermal distortion, certain DDM photos can't be ascribed to Earth. It estimated noise pixels in DDMs may be reduced this approach after filtering CYGNSS data. Figure 2 illustrates DDMs with and without estimated noise pixels.

Dielectric constants and land surface quality fluctuate during floods, therefore they may be used to determine whether flooding has transpired. The investigation extracts 7 DDMs connected towards the 2 factors as BPNN inputs. SR, PR, LES, leading advantage of slopes, PPP, DDM average (Tehrany *et al.*, 2013) and SNR (Geirhose *et al.*, 2019) (Figure 3).
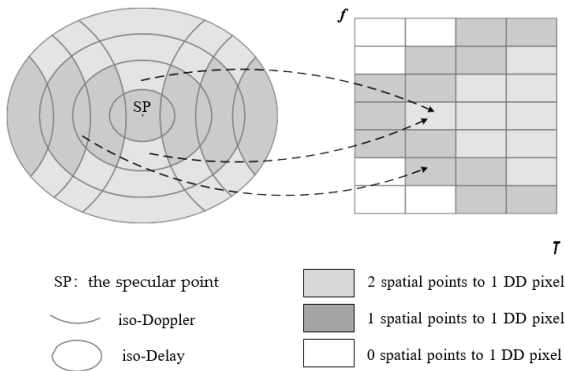
Figure 2. Analysis of the spatial co-ordinate system with delay-Doppler connection

A delay isoline is represented by the ellipse, while a doppler shift isoline is represented by the curves. The one and two measurement points in the left, particularly when studying, are represented by the blue and yellow postponed Doppler dots in DDMs, respectively. This is shown by the right simple adaption the painful reflection.
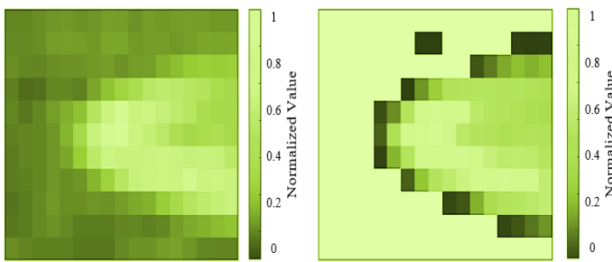
Figure 3. (a) DDMs before removing noise pixels; (b) DDMs after removing noise pixels

Table 2. Extraction of features from DDMs

Extraction of Symbol	Name of Features
Peak	The peak value of DDMs
SNR	Signal-to-Noise Ratio
PR	Power ratio
SR	Surface Reflectivity
LES	Leading Edge of Slope
TES	Tail edge Of the Slope
DDMA	Average of DDM

2.3. Creation of MNN model

The CNNs module, BP artificial neural subsystem, concatenation layer, physical hardware in its entirety, and a number of neurons are all parts of the MNNs model (Figure 4b) The CNNs module contains 16 and 32 *3 *3 convolutional filters and two layers.E very Gaussian kernels may be seen as a features extracted that combines with the receiving DDMs to create local features. For example, the kthCNN modelprocesses the input DDM to create the image representation $h_k^{(1)}$.

$$h_k^{(1)} = f\left(\left(W_k^{(1)} * X\right) + b_k^{(1)}\right) \qquad (1)$$

where the input is X The kth convolutional network's mass and biases are DM,Wk(1) and bk(1)., * symbolizes the convolution layer, and f signifies the activation function.

$$f(z) = maximum(0,z) \qquad (2)$$

In the CNN component, the maximum a 2*2 size allows for the most pooling. And a duration of 2 is used to subsample the image features that are obtained by the convolution operation. This is done to limit the amount of unnecessary data while maintaining the key features.

The BP module of the MNN paradigm is divided into two layers, each of which has 16 and 32 neurons. The signals are weighted and summarized by each neuron in the component, and the ReLU activation function then processes the results to produce an output feature. Consider, for instance, how the ith neuron FCs functions. $y_i^{(1)}$ may be described by the equation as results:

$$y_i^{(1)} = f\left(\sum 1\left(x_j \times w_{ij}^{(1)}\right) + b_i^{(1)}\right) \qquad (3)$$

X_j is the neuron's j^{th} input feature; $W_{ij}^{(1)}$ and $b_i^{(1)}$ are its weight and bias. The ReLU activation function is denoted by f().

CNN and BP characteristics are added to the concatenated layer. After being non-linearly analyzed by a layer of 64 neurons, aggregated characteristics are sent to the output neuron. Two softmax-activated neurons can be found in the hidden layers, which produce probabilities p_i of using DDM input that corresponds to submerging area of significant site locality. The following is an expression for the probability p_i:

The CNNs & BPs characteristics are added to the synthesis layer. Since being non - linearly analyzed by a level of 64 neurons, synthesized data are sent to the output units. Two neurons in the output nodes have the soft - max functional (Alzubaidi *et al.*, 2023; ehrany *et al.*, 2019; Tsubaki and Kawahara, 2013) and output probability p_i from the inputs DDMs that correlate to the immersed area and the significant sites region. The following is an expression for the likelihoods p_i:

$$p_i = \frac{\exp(v_i)}{\sum_{j=1}^{k} \exp(v_j)} \text{ where } i = 1,2 \qquad (4)$$

v 1 and v 2 are the inputs to the softmax function, and k is the frequency of the output layer neurons, set at 2. For

each classification, the softmax function in neural networks generates a set of probability values, and it should be kept in mind that the sum of all probability values is 1. The attribution category for the sample has the highest likelihood value. The proposed MNN framework only generates two probability values because it is a binary classification model. As a result, the linked subcategory is the categorization category if the probability is larger than 0.5. The sample distribution that corresponds to the flooded area may be chosen as the model's prediction outcome as the MNN model generates just two probability values, and their sum is 1, making this choice possible. therefore, samples with probability. Therefore, samples with probability values greater than 0.5 are regarded as hidden samples.
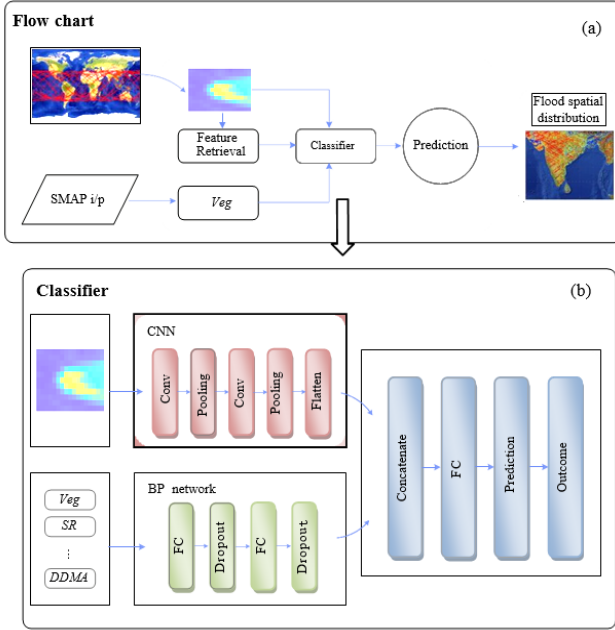
Figure 4. Flooding phase of the MNN; (b) MNNs layered view

2.4. Training MNNs for prediction

The database in this work is acquired through Spatio-temporal matching of SMAP statistics from May to September 2020 with CYGNSS data. A CYGNSS data will give, and a DDM 7 characteristics, as depicted SMAP values are shown in Table 3 provides vegetative characteristics and the source of the proposed label the different classifiers flooded vs non-flooded regions defined by SMAP moisture content (Wang *et al.*, 2018). In this work, 50,000 samples were selected picked from the database as the MNN model's training, verification, and evaluation subgroups.

These subgroups are intended to provide enough information training networks, assess effectiveness, similarly alter the hyperactive -parameters. The MNNs network for flood detection inverted predicts the remaining database items. MNN learning algorithm utilizes software forward propagating and error back-propagation. At forward propagate, the neural cable network settings stay unchanged, but in backward propagates, they are dynamically changed using the Adam optimizers to reduce the gradient descent. The model's error function is (5):

$$L = \frac{1}{M}\sum_{m=1}^{M}\sum_{k=1}^{K} y_m^k \times \log\left(h_\theta\left(x_m, k\right)\right) \qquad (5)$$

In this experiment, K is the number of classes, adjusted to 2. M is the number of training samples in each round; y_m^k is the objective label, in accordance with the SVM classifier of inundation vs non-inundated regions defined by SMAP moisture content [43]; X is the learning sample input, and $m; h_\theta$ is the weighted neural network model. The variables of the MNN algorithm are modified in accordance with the following formula throughout each training round:

$$\begin{cases} g = \nabla_\theta L \\ m = \beta_1 m + \left(1 - \beta_1\right)g \\ s = \beta_2 s + \left(1 - \beta_2\right)g^2 \\ \hat{m} = \dfrac{m}{1 - \beta_1^T} \\ \hat{s} = \dfrac{s}{1 - \beta_2^T} \\ \hat{\theta} = \theta - \eta m / \sqrt{s + \epsilon} \end{cases} \qquad (6)$$

where $\nabla\theta$ stands for the inclination operation, and "g" Lbe the inclination loss using the parameter θ; η is the learning stage, default of limit 0.001; m and S denoted as 1st, 2nd momentary factors β_1 and β_2 denotes the exponential decay coefficients of m and S; ϵ is a constant, set to 10^{-6}; t is the number of iterations.

Here's how the suggested MNN model is trained:

1. Set the neural platform's initialization settings and feed it with training data.

2. Carry out forward propagating and use Equations to determine the gradient descent (6).

3. Update the neural network settings using the backpropagation algorithm and Adam optimization.

4. When the loss density function's fluctuation is smaller than 0.001 throughout 10 epochs, or after the specified number of times, learning should be stopped.

## 2.5. Forecasting with MNNs techniques

The trained MNN model can be utilised as a classifier for flood monitoring. The procedure of monitoring floods is shown in Figures 5 and 6a. (1) CYGNSS data are entered into the MNN model to ascertain the odds that the CYGNSS data correspond to the submerged area. Particularly, areas with probabilities greater than 0.5 are considered to be submerged, whilst those with probabilities lower than 0.5 are considered to be non-submerged. (2) After combining the prediction outcomes with the location of DDMs, the scatter maps of the expected results are then produced. The longitude and latitude of each DDM's specular point are then used to determine its geolocation. (3) Images measuring 9 km are then created using the forecast findings' scatter maps that have been griddled.

2.6. Process for creating surface flowing feature

Images are made of colored pixels. The present study led to the creation of Surface Flowing Feature. In Table 2, landform analysis with soil characteristics are illustrates in geographical study results. These two sets of data are rasters, which implies that grids of numbers make up each one of them Figure 4 depicts the concept of expanding Surface Flowing Feature. Using moisture, land cover, and soil mapping factors, every grid's Surface Flowing Features is calculated. The grids may confound matrix calculation; matrix were computed one by one

2.7. Predicting flood feature based on rainfall

Thiessen polygons are used to determine hydrological flood. They create discontinuous rainfall differences since each polygon has a distinct estimate. Thiessen polygons have recurrent feature modification shapes, making them unsuitable for developing the Network model. The Thiessen polygons may be approximated spatially. Previous research has used the inverse distance weighted approach the kriging method and the spline method as instances of discretization. There are many possibilities for each approach, including regularized, co-kriging, universal, and basic geostatistical for the spatial interpolation technique.
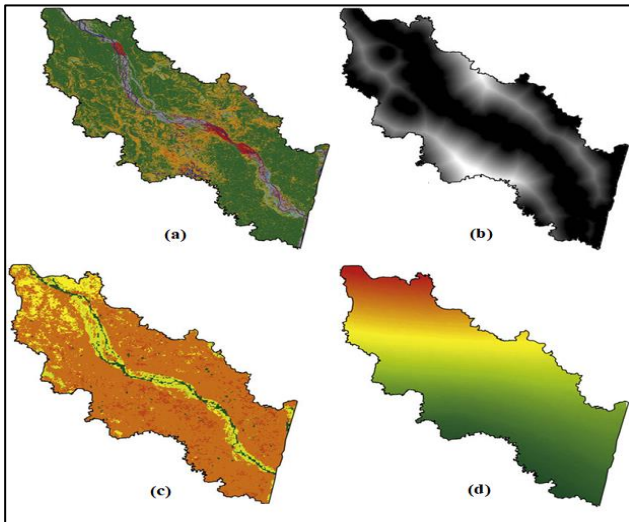
Figure 5. Diagrammatic view of (a) Land cover; (b) Surface feature; (c) Soil cover and (d) Rainy cover

There are many types of curvatures, including thin-plate curvatures, multi-quadratic, inverted multi-quadratic, and curves with tensors. IDW, on the other hand, lacks the extra possibilities offered by the aforementioned spatial interpolation approach while still having the benefits of a straightforward methodology and effective spatial interpolation implementation. Since the major focus of this research is the data-generating approach and its application, numerous spatial interpolation methods were deemed inappropriate. IDW was deemed most acceptable for reducing the impact of using the spatial interpolation method. IDW was used for spatial interpolation in this investigation. IDW is a geostatistical approach that allocates a weight based on Tobler's law of geographic. Since IDW assumes that the length between an observed point and a neighboring documented point is inverse

linked to the measurement values, it generates a greater range of forms than Thiessen polygons. To avoid the repetition of Thiessen polygon, grid-type precipitation systems are designed using IDW.

$$Z_x = \frac{\sum_{i-1}^{n}\left(w_i Z_{x_i}\right)}{\sum_{i=1}^{n} w_i}, w = \frac{1}{L_i^2} \qquad (7)$$

where Z_π is the estimated value of the unseen point, w_i is the weight, Z s is the utilization of the adjacent point, and L_i is the distance between the undetected and observable points.

2.8. Calculation of grid values in a specific feature

Every grids calculation from Figure 5 is computed that use the curve number CNs. It established by the Soil Conservation Service (SCS), this is the precursor of the U.S. National Resource Conservation Services, noted out the drawbacks of the scs curve CNs, such that "sensitivity to the choice of CNs," "lack of clear good description about a Pre-Moisture Condition - PMC" "change in CN for diverse biota," "lack of clear explanation regarding transformation in spatial level," that "ini Various research have shown the CN's use for hydrological study. The CN is calculated based on variables including rainfall, soil properties, and land cover. It is helpful for modeling streamflow and assessing hydrologic consequences. This research showed that the CNs can be employed in SURFACE FLOWING FEATURE production, given its application in hydrologic evaluation.

Rainfall (P) and remaining sufficient water (S, Eq. 8) are used to compute CN to determine watershed runoff (Q). When creating SURFACE FLOWING FEATURE, the same numerical process used to produce CNs is used, but Q is determined for every grid instead of just one CN for the whole watersheds. Additionally, every grid's determined Q is set as a dimensionless number without regard to the unit.

$$Q = \frac{(P-0.2S)^2}{(P+0.8S)}\left(P \geq I_2, I_1 = 0.2S\right) \qquad (8)$$

$$Q = 0\left(P < I_2, I_a = 0.2S\right) \qquad (9)$$

$$S = \frac{25400}{CN} - 254 \qquad (10)$$

The grid ratio in Eq. (8) is significantly influenced by the CN. It is given due to the physical traits and situations of the 4 distinct kinds of coils that make up Hydrologic Soil Groups (HSG) A, B, C, as well as D. The SCS gives CN values as a list, however they are incorrect for South Korea due to geographical differences. The Ministries of Land, Construction, and Transportation of South Korea advises utilizing these CN. So, using the soil maps & forest cover map that the DFET of a Department of Land, Building, and Transportation gave, the current study's CNs of the research region were calculated.

The SCS suggests modifying CN 1 (CN 1, Eq. (9)) and CN II (CNIII, Eq. (10)) to take preceding rainfalls into account.

The preceding rainfall is used to determine the soil moisture of the surface in order to the downpour and increase in direct runoff after the saturate. The straight-line approach, the N-day method, and the stream flow regression curve are the examples of standard approaches that might be suggested for direct runoff and base flow based on the rainfall that came before it. However, these technologies only provide 1D data that is relevant to the whole watershed, making it challenging to extend the data into the 2D kind of data needed for SURFACE FLOWING FEATURE. Antecedent rainfall suggested in the SCS-CN may be employed in place of the aforementioned approaches in this research, and it can be effectively used to create SURFACE FLOWING FEATURE. The SCS-CN approach takes into account the PMC impact in accordance with the antecedent rainfall. In this context, antecedent rainstorms refer to the runoff's 5-day total precipitation (P5). Dry and wet seasons and three stages, PMCI, II, and III, may be used to categorize the PMC. As advised by the SCS, the grid value was determined using the PMC in daily units. The dry and wet seasons are stated to run from Oct to May & Jun to Sept.according to the weather of Korea. The daily PMC was found by computing the daily P5, and the daily modified CN were derived.

$$CN_1 = \frac{4.2CN_{11}}{10 - 0.058CN_{II}} \sum\nolimits_{i-1}^{5} P_i \text{ Space in front of summation for sum}$$

$$P \begin{cases} < 12.7mm(\text{dry season}) \\ < 35.6mm(\text{wet season}) \end{cases} \tag{11}$$

$$CN_{ml} = \frac{23CN_{II}}{10 + 0.13CN_{II}} \sum CN_{i-1}^{5} P_i \text{ Space in front of summation for sum}$$

$$\{ > 27.9mm(\text{dry season}) > 53.3mm(\text{wet season}) \} \tag{12}$$

2.9. Surface flowing features prediction

The Surface Flowing Feature utilizing Eqs. (11) & (12) would not reflect any spatial patterns in dry situations since Q of each grid turns zero if rainfall is 0 or less than

efficient rainfall (Ia). For this investigation, both dry and wet circumstances must be simulated. The Surface Flowing Feature is only suitable for wet circumstances, therefore everyday runoff modeling is not feasible with it. As a result, characteristics other than the Surface Flowing Feature, which represents the weather, are necessary. An approach is to take into account a river's drainage during a dry spell. In natural rivers, drainage often continues even in dry weather. This suggests that the base stream determines stream flows and that runoff during dry periods is reliant on groundwater. In many earlier studies, the base flow is believed to be groundwater, and research have explored underground water budget or recharge. In this research, the runoff increase during dry situations. To describe the spatial changes in groundwater table by attributes, spatial analysis is conducted using the information at the site where the water depth is collected, together with IDW. Base flows are grid features with the same precision as land coverage and soil maps.
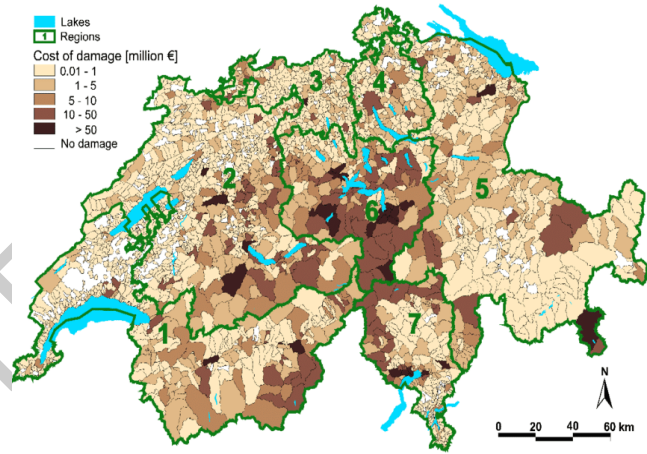
Figure 6. Catchment areas' geographic distributions for trained data (green outline), validating statistics, and testing datasets (brown fills)

Table 3. Categorization of the PMC

PMC	Season in Dry	Season in Wet
Condition in Dry	Ps lesser than 12.7	Ps lesser than 35.6
Condition in Wet	Ps greater than 27.9	Ps greater than 53.3
Condition in Normal	127 less than equal to Ps less than 27.9	35.6 lesser than Ps lesser than 53.3

2.10. Numerical results in catchment region

The elevation data for this investigation were obtained from the ETH Zurich GeoVITegeodata service (https://geovite.ethz.ch/). Uploaded information was transformed into catchment regions using GIS software. Elevation information comes from two areas. The first region is around Zurich, Switzerland, and has 750 catchment areas. Switzerland's Lausanne and Geneva have seven catchment regions. The first region's catchments were divided into two groups at arbitrary, each of which has 500 and 200 catchments. The bigger set served as a training sample, whereas the smaller set served as a validation set. The testing set included all

second-region catchments. Catchment regions with red limits indicate they are part of the verification and test databases in Figure 6, which depicts the geographical distribution of the information. The terrain features of the records are shown in Figure 7. These features reveal the average circumstances of the catchments, not precise geographic distribution. conv(n) indicates one convolution operation with the kernel size set to 3, convp(n) uses two CNNs with the wireless router's specified kernel size and one maximum pooling layer; n is the quantity of image data, and Upconv(n) is a convolution layer with a gaussian kernel of 3 and one up-sampling layer. When doing the training, catchment variables also weren't utilized as

inputs. All catchment areas' ground truth was produced to use the CADDIES system. The CADDIES flood model uses template matching and can simulate pluvial floods quite quickly. All five-hour scenarios were focused on a 100-year event developed utilizing alternating blocks. Note that this 100-year rainfall occurrence was applied over the whole area without understanding the local rainfall patterns.

An accuracy of 97.2 percent in flood susceptibility modeling is an impressive result that indicates the proposed methodology is performing very well in predicting flood-prone areas. Achieving such a high accuracy suggests that the model is effectively capturing the relationships between the input features (elevation data, socio-economic variables, and infrastructure data) and flood occurrences, allowing it to make accurate predictions.

The high accuracy of 97.2 percent implies that the model can correctly identify 97.2 percent of the flood-prone areas and non-flood-prone areas in the dataset. This indicates that the model is successfully distinguishing between the characteristics of flood-affected catchment

regions and those that are less susceptible to flooding. Such accuracy can be beneficial in supporting decision-making processes related to flood risk assessment, disaster preparedness, and urban planning, as it helps identify areas that require special attention and investment in flood mitigation measures.
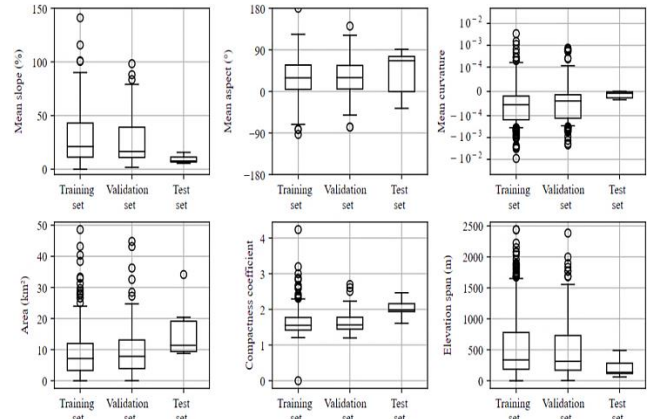

Figure 7. The training, validating, and test databases' geographical features

Table 4. Analyses utilised a 100-year rainfall data event

Intervals of Rainfall (minimum)	0 to 5	5 to 10	10 to 15	15 to 20	20 to 25	25 to 30	30 to 35	35to 40	40 to 45	45 to 50	50 to 55	55 to 60
Intensity of Rainfall (minimum/hr)	24.2	26.9	30.8	37.1	50.2	161.5	65.7	42.2	33.5	28.7	25.5	23.1

Table 5. The Evaluation metrics

Indicator	Equation	Limits	Value
D1	$$d_1 = 1 - \frac{\sum_{i-1}^{n} |y_i - y_i'|2}{\sum_{i-1}^{n}(|y_i - y| + |y_i'' - y|)}$$	[0,1]	1
RMSE	$$RMSE = \sqrt{\frac{\sum_{i-1}^{n}\left(y_i - y_i''\right)2}{n}}$$	[0, + infinity]	0

Table 6. Different models tested in the validation experiments

Name	Size of Input	Field of Receptive	Size of Kernel	Sequence of layer	Result
1027 k7 to 1027 k3	1027*1027	1588 572	73	convp(8); convp (16); convp(32); convp(64); convp (128); convp (256); 2 × conv (512); upconv (256); upconv (128); upconv (64); upconv(32); upconv(16); upconv(8); conv (2)	Both options
512 k7 to 512 k3	512*512	788 284	73	convp(16); convp (32); convp(64); convp(128); convp(256); 2 × conv(512); upconv(256); upconv(128); upconv(64); upconv(32); upconv(16); conv (2)	The patch based Options
256 k7- 256 k3	256*256	388 140	7 3	convp(32); convp (64); convp(128); convp(256); 2 × conv(512); upconv(256); upconv(128); upconv(64); upconv(32); conv (2)	-

Utilizing the same event serves the dual function of the primary component (terrace altitudes) while keeping additional statistical system in line Tables 4–6 shows the event's rainfall. Different preparation methods have been used to create the classification model for the patch- and resizing-based choices. The patch-based option uses input-output pairings randomly picked from of the learning dataset's coverage regions. The topography

altitudes, the greatest depth of water, and the highest velocity distribution are all represented by vector maps in each patch. In order to make the patch pixels 3 times as many as the pool pixels, we sampled at a rate the patches. For the resizing-based approach, classification model were raster maps of resized catchment regions. In order to accommodate CNN input size, the feature was placed in the centre of the larger of the two actual intake regions,

while the smaller of the two output regions was filled with 0s. Additionally, inputs were rotated and flipped to optimise training data. The training dataset was used to train the CNN models, while the validation and testing datasets were used to evaluate them. Training data was handled in both scenarios before being fed to convolutional networks. Three phases comprise the pre-processing stage:1) Slope, perspective, and curve computation using raw elevation data 2) scaling the raw elevation x_{raw} to a constant $c(max\ x_{raw})$, where max offers the greatest advantage; and 3) combining

topographic information and the elevation that has been downscaled to produce raster maps with several picture channels. Every pixel that was empty during the data preparation was changed to have a value of 0. In spite of the fact that the CNNs may have learned and converged using raw topographic maps, our research shows that learning was significantly faster using preprocessed training data. The test findings also showed that choosing the appropriate option surpassed learning effectiveness and lower values of c, such as 0.01 in range.

Table 7. Comparison of proposed model against existing works

Model Type	Advantages	Disadvantages
MNN (Proposed Model)	Spatio-Temporal Accuracy: Utilizes forthcoming GNSS technology for precise dynamic flood monitoring.	Data Dependency: Relies on availability and quality of GNSS and SMAP data.
	Reduced Processing Time: CNN-based approach speeds up processing compared to traditional models.	Training Complexity: Building and training the MNN model may require more computational resources.
	Automatic Feature Extraction: CNN extracts abstracted features from images and incorporates GNSS characteristics.	
Statistical Models	Simplicity: Easy to implement and understand.	Difficulty in Capturing Complexity: Struggles with capturing complex spatial patterns and nonlinear relationships.
	Reliance on Historical Data: Uses historical flood occurrence data and spatial attributes for prediction.	
Machine Learning Models	Flexibility: Better handling of nonlinear relationships compared to statistical models.	Feature Engineering: Performance depends on manual feature engineering and parameter selection.
	Improved Prediction Accuracy: Can capture complex patterns.	

The Table 7 summarizes the advantages and disadvantages of each model type. The MNN model shows strengths in spatio-temporal accuracy, reduced processing time, and automatic feature extraction. As, its effectiveness depends on data availability and training complexity. Statistical models are simple and rely on historical data but struggle with complexity. Machine learning models offer flexibility and improved prediction accuracy but require feature engineering and parameter tuning. Understanding these trade-offs is essential for selecting the proposed model for flood susceptibility mapping in different scenarios.

3. Discussion

The presented study focuses on flood susceptibility modeling using a Multi-layer Neural Network (MNN) as the core architecture. The MNN incorporates convolutional and up-sampling layers to capture complex spatial and temporal patterns related to flood occurrences. The results demonstrate an impressive accuracy of 97.2 percent, indicating the effectiveness of the proposed methodology in predicting flood-prone areas. The high accuracy suggests that the model effectively leverages the input features, including elevation data, socio-economic variables, and infrastructure data, to distinguish between flood-affected catchment regions and those less susceptible to flooding. Such accurate predictions are valuable for supporting flood risk assessment, disaster preparedness, and urban

planning, enabling identification of areas requiring targeted flood mitigation measures. The use of forthcoming GNSS technology for precise dynamic flood monitoring enhances the MNN's spatio-temporal accuracy and reduces processing time through CNN-based feature extraction. However, the dependence on GNSS and SMAP data poses a challenge, as data availability and quality may vary across different regions and times. Additionally, the training complexity of the MNN requires significant computational resources, necessitating careful consideration of resource constraints for practical implementation.

To address model interpretability concerns often associated with deep learning models, the study introduces novel methods based on statistical analysis of the derivatives of the model's outputs with respect to each hidden neuron. These methods quantify the contribution of individual neurons, shedding light on the learned features' significance and aiding in understanding the MNN's decision-making process. This interpretability aspect enhances the model's transparency and facilitates better-informed decision-making, especially in critical scenarios. The comparison of the proposed MNN model with existing statistical and machine learning models highlights its advantages in spatio-temporal accuracy, reduced processing time, and automatic feature extraction. However, the trade-offs include data dependency on GNSS and SMAP, training complexity, and

the need for sufficient training data. Statistical models, while simple and interpretable, may struggle with capturing complex spatial patterns and nonlinear relationships. Machine learning models offer improved prediction accuracy and flexibility but require careful feature engineering and parameter tuning.

Thereby, the proposed flood susceptibility modeling methodology demonstrates promising results and offers valuable insights. The study's contributions lie in achieving high accuracy, leveraging GNSS technology, introducing interpretability methods, and comparing against various model types. Researchers and practitioners can leverage these findings to inform flood risk management strategies and enhance decision-making in flood-prone regions. However, future work should focus on addressing the data dependency aspect and investigating techniques for reducing training complexity without compromising accuracy to foster wider applicability of the proposed methodology.

4. Conclusion

In order to break the pattern of developing a CNN-based runoff model mostly based on meteorological data, an approach for producing surface feature and base flows data that reflect spatial attributes was developed. This research have looked into using these models to create new, quick applications for predicting fluvial but also pluvial floods, determining their extent, and determining their susceptibility to flooding. This study suggests a CNN component and a BP module-based MNN model for GNSS flood monitoring. The former is used to extract the DDMs' underlying abstract features, whilst the latter accepts input from GNSS-usual physical properties and vegetation data. This type of dual-branch neural network architecture allows the DBNN model to more effectively use GNSS information during flood inverting and dynamic tracking of floods. It can combine GNSS physical attributes with the abstract elements extracted by MNN. The studies' findings additionally demonstrated that neural network models with a broader receptive field typically display greater accuracy than systems with a smaller input vector. This implies that water retention is responsive to the catchment area's worldwide patterns and that the accuracy of predictions depends on the amount of global data available. The systematic encoding of catchment regions of arbitrary sizes and shapes will continue to be difficult. In our e future experiments, this problem was addressed resizing-based alternatives with self learning neural network models.

Credit authorship contribution statement

Swathika R: Formal analysis, Conceptualization, Methodology & Writing. Radha N: Investigation and Validation with review & editing

Declaration of Competing Interest

The authors declare that they have no known competing financial interests or personal relationships that could have appeared to influence the work reported in this paper.

References

Ahmed H., La H.M. and Tran K. (2020). Rebar detection and localization for bridge deck inspection and evaluation using deep residualnetworks. *Automation in Construction*, **120**, 103393

Akhtar M.K., Corzo G.A., van Andel S.J. and Jonoski A. (2009). River flow forecasting with artificial neural networksusing satellite observed precipitation pre-processed with flow length and travel time information: Casestudy of the Ganges river basin. *Hydrology and Earth System Sciences*, **13**, 1607–1618.

Alfieri L., Velasco D. and Thielen J. (2011). Flash flood detection through a multi-stage probabilistic warning system for heavy pre-cipitationevents, *Advances in Geosciences*, **29**, 69–75.

Ali H. and Choi J-H. (2019). A Review of Underground Pipeline Leakage and Sinkhole Monitoring Methods Based on Wireless SensorNetworking. *Sustainability*, **11**, 4007

Alzubaidi L., Bai J., Al-Sabaawi A., Santamaría J., Albahri A.S., Al-dabbagh B.S.N. and Gu Y. (2023). A survey on deep learning tools dealing with data scarcity: definitions, challenges, solutions, tips, and applications. *Journal of Big Data*, **10**(1), 46

Amit S.N.K.B. and Aoki Y. (2017). Disaster Detection from Aerial Imagery with Convolutional Neural Network, In Proceedings of the 2017International Electronics Symposium on Knowledge Creation and Intelligent Computing (IES-KCIC), Surabaya, Indonesia, 26–27September 2017, 239–245.

Anusha N. and Bharathi B. (2020). Flood detection and flood mapping using multi-temporal synthetic aperture radar and optical data.*Egyptian Journal of Remote Sensing and Space Science*, **23**, 207–219

Baatz M. and Schäpe A. (2000). Multiresolution Segmentation, An Optimization Approach for High Quality Multiscale Image Segmentation. In Angewandte Geographische Informations verarbeitung, WichmannVerlag, Karlsruhe, Germany, 12–23.

Basha E. and Rus D. (2007). Design of early warning flood detection systems for developing countries. In Proceedings of the 2007 InternationalConference on Information and Communication Technologies and Development, Institute of Electrical and ElectronicsEngineers (IEEE), Bangalore, India, 15–16 December 2007; 1–10.

Castelluccio M., Poggi G., Sansone C. and Verdoliva L. (2015). Land use classification in remote sensing images by convolutional neural networks. arXiv, arXiv:1508.00092.

Chen P.A., Chang L.C. and Chang F.J. (2013). Reinforced recurrent neural networks for multi-step-ahead flood forecasts. *Journal of hydrology*. **497**, 71–79. https://doi.org/10.1016/j. jhydrol.2013.05.038.

Di Martino G., Iodice A., Riccio D. and Ruello G. (2007). A Novel Approach for Disaster Monitoring: Fractal Models and Tools. *IEEE Transactions on Geoscience and Remote Sensing*, **45**, 1559–1570.

Ejaz W., Ahmed A., Mushtaq A. and Ibnkahla M. (2020). Energy-efficient task scheduling and physiological assessment in disastermanagement using UAV-assisted networks, *Computer Communications*, **155**, 150–157

Elsafi S.H. (2014). Artificial Neural Networks (ANNs) for flood forecasting at Dongola Station in the River Nile, Sudan. *Alexandria Engineering Journal*, **53**, 655–662.

Felli F., Liu C., Ullah F. and Sepasgozar S. (2018). Implementation of 360 videos and mobile laser measurement technologies for immersivevisualisation of real estate & properties, In Proceedings of the 42nd AUBEA Conference, Singapore, 26–28 September 2018.

Fu G., Liu C., Zhou R., Sun T. and Zhang Q. (2017). Classification for High Resolution Remote Sensing Imagery Using a Fully ConvolutionalNetwork. *Remote Sens*, **9**, 498.

Geirhos R., Rubisch P., Michaelis C., Bethge M., Wichmann F.A. and Brendel W. (2019). ImageNet-trained CNNs are biased towards texture; increasing shape bias improves accuracy and robustness. In: 7th International Conference on Learning Representations (ICLR 2019). New Orleans, USA. Oral presentation. https://openreview.net/forum?id=Bygh9j09KX.

Gers F.A., Schmidhuber J. and Cummins F. (1999). Learning to forget, Continual prediction with LSTM, In Proceedingsof the 9th International Conference on Artificial Neural Networks (ICANN) 99, Edinburgh, UK, 7–10 September, 9, 850–855.

Hitokoto M., Sakuraba M. and Sei Y. (2016). Development of the real-time river stage prediction method usingdeep learning. *Journal, Japan Society of Civil Engineers, JSCE Ser. B1 Hydraulic, Engineering*, **72**, I_187–I_192

Hochreiter P. and Schmidhuber J. (1997). Long short-term memory. *Neural Computing*, **9**, 1735 1780.

Hochreiter S. (1998). The vanishing gradient problem during learning recurrent neural nets and problem solutions. *International Journal of Uncertainty Fuzziness Knowledge-Based Systems*, **6** (02), 107–116. https://doi.org/10.1142/S0218488598000094

Hosseiny H., Nazari F., Smith V. and Nataraj C. (2020). A Framework for Modeling Flood Depth Using a Hybrid of Hydraulics and Machine Learning, *Scientific Reports*, **10**, 1–14

Hu C., Wu Q., Li H., Jian S., Li N. and Lou Z. (2018). Deep learning with a long short-term memory networksapproach for rainfall-runo_ simulation, *Water*, **10**, 1543.

Islam A. and Shin S.Y. (2020). A blockchain-based secure healthcare scheme with the assistance of unmanned aerial vehicle in In-ternet ofThings, *Computers and Electrical Engineering*, **84**, 106627.

Ji S., Xu W., Yang M. and Yu K. (2013). 3D Convolutional Neural Networks for Human Action Recognition. IEEE Trans. Pattern *Anal. Mach.Intell*, **35**, 221–231.

Jozdani S.E., Johnson B.A. and Chen D. (2019). Comparing Deep Neural Networks, Ensemble Classifiers, and Support Vector MachineAlgorithms for Object-Based Urban Land Use/Land Cover Classification. *Remote Sens*, **11**, 1713

Kastridis A., Kirkenidis C., Sapountzis M. (2020). An integrated approach of flash flood analysis in ungauged Mediterranean watershedsusing post-flood surveys and Unmanned Aerial Vehicles (UAVs), *Hydrological Processes*

Kensert A., Harrison P.J. and Spjuth O. (2019). Transfer learning with deep convolutional neural networks forclassifying cellular morphological changes. *SLAS Discove*r, **24**, 466–475.

Khosravi K., Panahi M., Golkarian A., Keesstra S.D., Saco P.M., Bui D.T. and Lee S. (2020). Convolutional neural network approach forspatial prediction of flood hazard at national scale of Iran. *Journal of Hydrology*, **591**, 125552

Kolar Z., Chen H. and Luo X. (2018). Transfer learning and deep convolutional neural networks for safety guardraildetection in 2D images. *Automation in Construction*, **89**, 58–70.

Kratzert F., Klotz D., Shalev G., Klambauer G., Hochreiter S., Nearing G. (2019). Towards learning universal, regional, and local hydrological behaviors via machine learning applied to large-sample datasets. *Hydrology and Earth System Sciences*. **23** (12), 5089–5110.

Kumar S.J., Kumar S., Choksi M. and Zaveri M.A. (2020). Collaborative data acquisition and processing for post disaster manage-mentand surveillance related tasks using UAV-based IoT cloud, *International Journal of Ad Hoc and Ubiquitous Computing*, **34**, 216–232.

Laptev N., Yu J. and Rajagopal R. (2018). Reconstruction and regression loss for time-series transfer learning.In Proceedings of the Special Interest Group on Knowledge Discovery and Data Mining (SIGKDD) and the4th Workshop on the Mining and LEarning from Time Series (MiLeTS), London, UK, 20 August 2018

Le X., Ho H.V., Lee G. and Jung S. (2019). Application of long short-term memory (LSTM) neural network forflood forecasting, *Water*, **11**, 1387

LeCun Y., Bottou L., Bengio Y. and Ha_ner P. (1998). Gradient-based learning applied to document recognition. *Process. IEEE*, **86**, 2278–2324.

Leit˜ao J.P., Zaghloul M. and Moosavi V. (2018). Modelling overland flow from local inflows in "almost no-time" using Self-Organizing Maps. In: 11th International Conference on Urban Drainage Modelling, Palermo, Italy. Oral presentation.

Liu W., Chen Z. and Zheng M. (2020). An Audio-Based Fault Diagnosis Method for Quadrotors Using Convolutional Neural Network andTransfer Learning. In Proceedings of the 2020 American Control Conference (ACC), Denver, CO, USA, 1–3 July 2020.

Long J., Shelhamer E. and Darrell T. (2015). Fully convolutional networks for semantic segmentation. In: Proceedings of the 28th IEEE conference on computer vision and pattern recognition (CVPR 2015). Boston, USA, 3431–3440. doi: 10.1109/ CVPR.2015.7298965.

Lopez-Fuentes L., Van deWeijer J., Bolanos M., Skinnemoen H. (2017). Multi-modal deep learning approach for flood detection. In Proceedings of the MediaEval 2017 Workshop, Dublin, Ireland, 13–15.

Maier H.R., Jain A., Dandy G.C. and Sudheer K.P. (2010). Methods used for the development of neural networksfor the prediction of water resource variables in river systems: Current status and future directions.Environment. *modelling software*, **25**, 891–909.

Marmanis D., Wegner J.D., Galliani S., Schindler K. and Datcu M. and Stilla U. (2016). Semantic Segmentation of Aerial Images with an Ensemble of CNNs. ISPRS Ann. Photogramm. *Remote Sensing and Spatial Information Sciences*, **3**, 473–480.

Mason D.C., Speck R., Devereux B., Schumann G.J.P., Neal J.C., Bates P.D. (2010). Flood Detection in Urban Areas Using Ter-raSAR-X. *IEEE transactions on geoscience and remote sensing*, **48**, 882–894.

Mehallegue N., Djellab M. and Loukhaoukha K. (2020). Efficient Use of UAVs for Public Safety in Disaster and Crisis Management. *Wireless Personal Communications*, 1–12.

Miyazaki K. and Matsuo Y. (2017). Stock prediction analysis using deep learning technique. In Proceedings of the31st Annual Conference of the Japanese Society for Artificial Intelligence, Nagoya, Japan, 23–26 May 2017.(In Japanese).

Mousa M., Zhang X. and Claudel C. (2016). Flash Flood Detection in Urban Cities Using Ultrasonic and Infrared Sensors, *IEEE Sensors, Journal*, **16**, 7204–7216

Nevo S., Anisimov V., Elidan G., El-Yaniv R., Giencke P., Gigi Y., Hassidim A., Moshe Z., Schlesinger M., Shalev G. *et al.* (2018). ML for Flood Forecasting at Scale In Proceedings of the Thirty-Second AnnualConference on the Neural Information Processing Systems (NIPS), Montréal, QC, Canada, 3–8 December 2018;Available online: https://arxiv.org/pdf/1901.09583.pdf (accessed on 31 October 2019).

Nguyen T., Han J. and Park D-C. (2013). Satellite image classification using convolutional learning, In Proceedings of the 11th International, Conference of Numerical Analysis and Applied Mathematics 2013, Rhodes, Greece, 21–27 September 2011; AIP Publishing:Melville, NY, USA, 2237–2240.

Potikyan N. (2019). Transfer Learning for Time Series Prediction. Available online: https://towardsdatascience.com/transfer-learning-for-time-series-prediction-4697f061f000 (accessed on 31 October 2019).

Pratt L.Y. (1992). Discriminability-Based Transfer between Neural Networks. In Proceedings of the Conference ofthe Advances in NIPS 5, Denver, CO, USA, 30 November–3 December 1992, 204–211.

Preethi P. and Asokan R. (2019). A high secure medical image storing and sharing in cloud environment using hex code cryptography method—secure genius. *Journal of Medical Imaging and Health Informatics*, **9**(7), 1337–1345.

Preethi P. and Asokan R. (2019). An attempt to design improved and fool proof safe distribution of personal healthcare records for cloud computing. *Mobile Networks and Applications*, **24**(6), 1755–1762.

Preethi P. and Asokan R. (2020). Neural network oriented roni prediction for embedding process with hex code encryption in dicom images. In Proceedings of the 2nd International Conference on Advances in Computing, *Communication Control and Networking* (ICACCCN), Greater Noida, India, (18–19).

Preethi P. and Asokan R. (2021). Modelling LSUTE: PKE Schemes for Safeguarding Electronic Healthcare Records Over Cloud Communication Environment. *Wireless Personal Communications*, **117**(4), 2695–2711

Preethi P., Asokan R., Thillaiarasu N. and Saravanan T. (2021). An effective digit recognition model using enhanced convolutional neural network based chaotic grey wolf optimization. *Journal of Intelligent and Fuzzy Systems*, (Preprint), 1-11.

Realestate Blog: The Worst Disasters Caused by Heavy Rain and Typhoons in Japan: 2011 to 2018.Available online: https://resources.realestate.co.jp/living/the-top-disasters-caused-by heavy-rain-andtyphoons-in-japan-2011-to-2018/ (accessed on 31 October 2019).

Rottondi C., Malandrino F., Bianco A., Chiasserini C.F. and Stavrakakis I. (2021). Scheduling of emergency tasks for multiservice UAVs inpost-disaster scenarios. *Computer Networks*, **184**, 107644

Salas F.R., Somos-Valenzuela M.A., Dugger A., Maidment D.R., Gochis D.J., David C.H., Yu W., Ding D., Clark E.P. andNoman N. (2018). Towards real-time continental scale streamflowsimulation in continuous anddiscrete space. *Journal of the American Water Resources Association. JAWRA* 2018, **54**, 7–27.

Sande V.C., Jong D.S. and Roo D.A. (2003). A segmentation and classification approach of IKONOS-2 imagery for land cover mapping toassist flood risk and flood damage assessment. *International Journal of applied earth observation and geoinformation*, 217–229.

Sankaranarayanan S., Prabhakar M., Satish S., Jain P., Ramprasad A., Krishnan A. (2020). Flood prediction based on weatherparameters using deep learning. *Journal of Water and Climate Change*, **11**, 1766–1783.

Sherrah J. (2016). Fully Convolutional Networks for Dense Semantic Labelling of High-Resolution Aerial Imagery arXiv, *arXiv*, 1606.02585.

Simonyan K. and Zisserman A. (2014). Two-stream convolutional networks for action recognition in videos. In Proceedings of the NIPS'14:Proceedings of the 27th International Conference on Neural Information Processing Systems, Montreal, QC, Canada, 8–13December 2014.

Smith L., Liang Q., James P. and Lin W. (2017). Assessing the utility of social media as a data source for flood risk management using areal-time modelling framework: Assessing the utility of social media for flood risk management, *Journal of Flood Risk Management*, **10**, 370–380

Suzuki T., Kim S., Tachikawa Y., Ichikawa Y. and Yorozu K. (2018). Application of convolutional neural networkto occurrence prediction of heavy rainfall, *Journal, Japan Society Civil, Engineering JSCE Ser, B1 Hydraulic. Engineering*, **74**, I_295–I_300, (In Japanese)

Tan Q.F., Lei X.H., Wang X., Wang H., Wen X., Ji Y., Kang A.Q. (2018). An adaptive middle and long-term runoff forecast model using EEMD-ANN hybrid approach. *Journal of hydrology*, **567**, 767–780. https://doi.org/10.1016/j.jhydrol.2018.01.015.

Te Chow V., Maidment D.R., Mays L.W. (1988). Applied Hydrology, *McGraw-Hill*. ISBN: 0-07-100174-3.

Tehrany M.S., Jones S. and Shabani F. (2019). Identifying the essential flood conditioning factors for flood prone area mapping using machine learning techniques. *Catena* **175**, 174–192. https://doi.org/10.1016/j.catena.2018.12.011.

Tehrany M.S., Pradhan B. and Jebur M.N. (2013). Spatial prediction of flood susceptible areas using rule based decision tree (DT) and a novel ensemble bivariate and multivariate statistical models in GIS. *Journal of hydrology*. **504**, 69–79. https://doi.org/ 10.1016/j.jhydrol.2013.09.034.

Tokar A.S. and Markus M. (2000). Precipitation-runo_ modeling using artificial neural networks and conceptual moldes. *Journal of Hydrologic Engineering*, **5**, 156–161.

Tsubaki R. and Kawahara Y. (2013). The uncertainty of local flow parameters during inundation flow over complex topographies with elevation errors. *Journal of Hydrology*, **486**, 71–87. https://doi.org/10.1016/j.jhydrol.2013.01.042.

Ullah F., Sepasgozar S.M.E. and Wang C. (2018). A Systematic Review of Smart Real Estate Technology: Drivers of, and Barriers to, the Useof Digital Disruptive Technologies and Online Platforms. *Sustainability*, **10**, 3142

Visual Geometry Group. (2019). Department of Engineering Science, University of Oxford, Available online: http://www.robots.ox.ac.uk/~{}vgg/research/very_deep/ (accessed 31 October 2019)

Wang Y., Chen A., Fu G., Djordjevic S., Zhang C. and Savi´c D.A. (2018). An integrated framework for high-resolution urban floodmodelling considering multiple information sources and urban features, *Environmental modelling and software*, **107**, 85–95

Wang Y., Chen A.S., Fu G., Djordjevi´c S., Zhang C. and Savi´c D.A. (2018). An integrated framework for high-resolution urban flood modelling considering multiple information sources and urban features. *Environmental modelling & software* **107**, 85–95. https://doi.org/10.1016/j.envsoft.2018.06.010.

Xue G., Liu S. and Ma Y. (2021). A hybrid deep learning-based fruit classification using attention model and convolution autoencoder.Complex & Intelligent Systems, 1–11, *Sustainability*, **13**, 7547 22 of 22

Yamada K., Kobayashi Y., Nakatsugawa M. and Kishigami J. (2018). A case study of flood water level prediction inthe Tokoro River in 2016 using recurrent neural networks, *Journal, Japan, Society, Civil. Engineering, JSCE Ser, B1 Hydraulic. Enginerring*, **74**, I_1369–I_1374, (In Japanese).

Ye H., Wu Z., Zhao R.-W., Wang X., Jiang Y.-G., Xue X. (2015). Evaluating Two-Stream CNN for Video Classification, In Proceedings of the 5th ACM on International Conference on Multimedia Retrieval, Association for Computing Machinery (ACM), Shanghai, China, 23–26 June 2015, 435–442.

Zeiler M.D. and Fergus R. (2014). Visualizing and under-standing convolutional networks. In Computer Vision—ECCV 2014; Fleet D., Pajdla T., Schiele B., Tuytelaars T., Eds.; *Springer International Publishing:Cham, Switzerland*, 818–833.

Zha S., Luisier F., Andrews W., Srivastava N. and Salakhutdinov R. (2015). Exploiting Image-trained CNN Architectures for UnconstrainedVideo Classification, In Proceedings of the British Machine Vision Conference 2015, Swansea, UK, 7–10 September; *British Machine Vision Association: Swansea*, UK, **60**.1–60.13.

Zhao G., Pang B., Xu Z., Peng D. and Zuo D. (2020). Urban flood susceptibility assessment based on convolutional neural networks. *Journal of Hydrology*, **590**, 125235.

Zhao Y., Wang T., Zhang S. and Wang Y. (2020). Towards minimum code dissemination delay through UAV joint vehicles for smart city.*IET Communications*, **14**, 2442–2452.